


Properties of Composite Electrodes for All-solid-state Fluoride-ion Secondary Batteries Processed by High-pressure Torsion



Yanchang WANG,^{a,§§} Sangmin LEE,^b Kentaro YAMAMOTO,^{a,c,*§}  Toshiyuki MATSUNAGA,^{a,§}
Hidenori MIKI,^{d,§} Hideki IBA,^{d,§} Koichi TSUCHIYA,^b Tomoki UCHIYAMA,^{a,§}
Toshiki WATANABE,^{a,§} Tsuyoshi TAKAMI,^{a,§} and Yoshiharu UCHIMOTO^{a,§§§}

^a Graduate School of Human and Environmental Studies, Kyoto University, Yoshida-nihonmatsu-cho, Sakyo, Kyoto 606-8501, Japan

^b Research Center for Structural Materials, National Institute for Materials Science, 1-2-1 Sengen, Tsukuba, Ibaraki 305-0047, Japan

^c Faculty of Engineering, Nara Women's University, Kitaouya-nishimachi, Nara 630-8263, Japan

^d Toyota Motor Corporation, Advanced Material Engineering Division, Higashifuji Technical Center, 1200 Mishuku, Susono, Shizuoka 410-1193, Japan

* Corresponding author: k.yamamoto@cc.nara-wu.ac.jp

ABSTRACT

All-solid-state fluoride-ion batteries (FIBs) using metal/metal fluorides are expected to be the next generation of storage batteries because they exhibit high volumetric energy densities by utilizing multielectron reactions, compared to the current lithium-ion batteries. However, method of fabricating a composite electrode for all-solid-state fluoride-ion batteries has not yet been established. A fabrication method for a composite electrode that disperses the active material and solid electrolyte is required. To approach this problem, in this study, we employed a high-pressure torsion (HPT) method, in which an active material, solid electrolyte, and conductive agent can be mixed with size reduction, as a new process and prepared Cu (active material)/PbSnF₄ (solid electrolyte)/acetylene black (conductive agent) cathode composites. The crystalline sizes of Cu and PbSnF₄ were significantly reduced. The apparent grain boundary resistance was also reduced owing to the more homogeneous distribution in the cathode composites after HPT processing. These structural and morphological changes led to high electrochemical performances, compared to a cathode composite without HPT.

© The Author(s) 2022. Published by ECSJ. This is an open access article distributed under the terms of the Creative Commons Attribution 4.0 License (CC BY, <http://creativecommons.org/licenses/by/4.0/>), which permits unrestricted reuse of the work in any medium provided the original work is properly cited. [DOI: [10.5796/electrochemistry.22-00133](https://doi.org/10.5796/electrochemistry.22-00133)].



Keywords : All-solid-state Fluoride-ion Batteries, Composite Electrode, High-pressure Torsion

1. Introduction

Reducing carbon dioxide emissions is a crucial issue that must be addressed to realize a sustainable society. Full-scale diffusion of electric vehicles (EVs) is required to achieve this goal. As the mainstream power source of EVs, the current lithium-ion batteries (LIBs) are approaching their theoretical limitation in terms of volumetric energy density, and thus it is essential to improve the volumetric energy density of rechargeable batteries for popularity of EVs.¹⁻³

To address the demand for batteries with high energy and power densities, a series of candidates that employ Na⁺, K⁺, Mg²⁺, Zn²⁺, Al³⁺, F⁻, or Cl⁻ as charge carriers have been developed.⁴⁻¹¹ Among them, all-solid-state fluoride-ion batteries (FIBs) using fluoride ions as carriers have attracted widespread attention because of the high volumetric energy density and safety.¹¹⁻¹⁷ In all-solid-state FIBs, metal/metal fluoride electrodes such as Cu/CuF₂ and Bi/BiF₃ can achieve large capacities using multielectron reactions (Bi/BiF₃: 385 mA h g⁻¹ to Bi; Cu/CuF₂: 843 mA h g⁻¹ to Cu).¹¹ Therefore, it is theoretically possible to achieve a high volumetric energy density over 5000 Wh L⁻¹,¹⁵ which significantly exceeds that of LIB-based systems, by employing combinations of appropriate cathodes and anodes. To fabricate the composite electrode for this battery, the metal active material and solid electrolyte fluoride must be mixed

uniformly for the discharge-initiated battery. However, method for this purpose has not yet been established.

It has been reported that diffusion length reduction of fluoride ions in the active material¹⁶ and formation of a good fluoride-ion path in the composite electrode¹⁸ are effective approaches to overcome these problems using thin-film model batteries.^{15,19} However, for bulk-type battery fabrication, it is necessary to establish a process that can produce fine particles of a powdered active material and form good fluoride-ion paths in the composite electrode. Hence, in this study, we focused on high-pressure torsion (HPT) processing, which can effectively refine metal grains and mix metal grains with other materials through the high shear stress generated during the processing,^{20,21} and used this method to prepare Cu/PbSnF₄ solid electrolyte/acetylene black (AB) cathode composites for all-solid-state fluoride batteries. The HPT treatment is effective to prepare refined Cu and PbSnF₄ particles and uniformly mixed Cu/PbSnF₄/AB cathode composites, which exhibit excellent electrochemical properties. We believe that the HPT treatment will be an important process technology in the preparation of composite electrodes with excellent electrochemical performances for FIBs.

2. Experimental

2.1 Material preparation

A commercial Cu nano powder (99.8%, US Research Nano-materials) was used as an active material. A PbSnF₄ solid electrolyte was prepared by a conventional solid-state reaction.¹⁷ Stoichiometric amounts of PbF₂ (99.9%, Kojundo, Japan) and SnF₂ (99%, Kojundo, Japan) were thoroughly ground using an agate mortar,

[§]ECSJ Active Member (Individual Member and person who belongs Corporate Member)

^{§§}ECSJ Student Member

^{§§§}ECSJ Fellow

K. Yamamoto  orcid.org/0000-0002-8739-4246

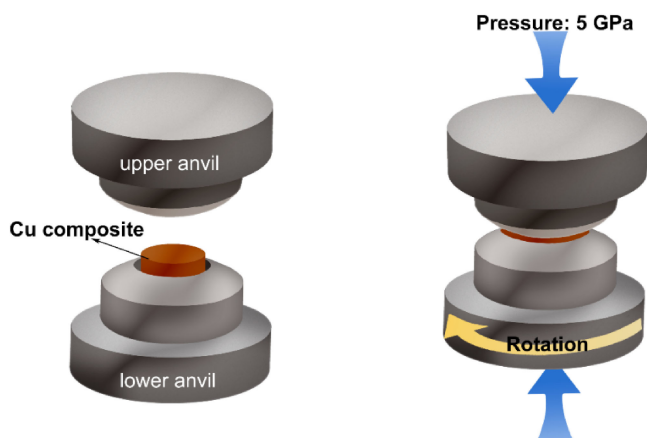


Figure 1. Schematic of the HPT process.

and then transferred to a ZrO₂ pod in an Ar-filled glove box. The mixture was milled using planetary ball mills (Fritsch Pulverisette7 premium line, Germany) with a rotation speed of 600 rpm for 12 h. The ball-milled mixture was transferred to the glove box and sintered at 400 °C for 1 h. A cathode composite was prepared by mixing the Cu nano powder, PbSnF₄ solid electrolyte, and AB, pre-dried under vacuum, in a mass ratio of 40 : 55 : 5 by ball milling at 100 rpm for 12 h. The as-prepared cathode composite was pressed into pellets under 180 MPa for 3 min for HPT processing.

2.2 HPT process

The HPT processing illustrated in Fig. 1 could introduce large shear strains on a disk-shaped sample.²² A disk sample with a diameter of 10 mm and thickness of approximately 1 mm was placed between two anvils. A high pressure, typically 5 GPa, was then applied. The lower anvil was rotated under the high pressure. The sample was slightly thicker than the recess on the anvils. A part of the sample flows out into the space between the anvils, which seals the sample. Thus, the sample can be deformed under a quasi-hydrostatic pressure, which minimizes the cracking during straining. In this study, disk pellets of the cathode composite were prepared by cold compaction. They were deformed by HPT under an applied pressure of 5 GPa with an anvil rotation speed of 1 rpm. The number of anvil rotations (N) was 5, 10, 20, 30, and 50. The cathode composites subjected to different N of HPT are hereafter referred to as HPT-0, 5, 10, 20, 30, and 50.

2.3 X-ray diffraction (XRD), scanning electron microscopy (SEM), and energy-dispersive X-ray (EDX) spectroscopy mapping

XRD patterns of the cathode composite after HPT with different rotation numbers were acquired using an XRD instrument (Rigaku Ultima IV, Japan) with CuK_α radiation ($\lambda = 1.54056 \text{ \AA}$). The microstructures of cross sections of the cathode composites after HPT with different rotation numbers were observed. The cathode composites were cut into half, mounted in the resin, and mechanically polished. Their morphological structures were observed using a Zeiss Auriga focused-ion beam (FIB)-SEM instrument with an operation voltage of 15 kV in the back-scattered electron mode. In addition, elemental mapping was performed using EDX spectroscopy with an EDAX Octane Elite instrument, equipped on the same FIB-SEM.

2.4 Electrochemical measurement

The ionic conductivities of the cathode composites after HPT processing with different rotation numbers were measured using an electron-blocking cell, as shown in Supplementary Fig. S1.^{23,24} The

cathode composite was placed into the cell and pressed with a pressure of 180 MPa for 3 min. The PbSnF₄ powder was then placed on the opposite side of the cathode composite pellet and pressed under a pressure of 180 MPa for 5 min. Electrochemical impedance spectra were acquired using a ModuLab XM ECS test system (Solartron Analytical) in the frequency range of 0.1 MHz to 10 mHz. The obtained data were fitted using the software ZView4 (Scribner and Associates).

An electrochemical measurement of each cathode composite was performed using a typical bulk-type cell. The PbSnF₄ powder was placed into the cell and pressed with a pressure of 90 MPa for 5 min. The cathode composite and Pb foil (99.9 %, Nilaco, Japan) were placed on the opposite side of the PbSnF₄ pellet and pressed under a pressure of 360 MPa for 5 min. Finally, the cathode composite/PbSnF₄/Pb foil was sandwiched by two pieces of Au foil as current collectors. A galvanostatic charge/discharge test was performed using an HJ1010SD8 (Hokuto Denko Corporation) electrochemical workstation. The cutoff voltage was set to 0.3–1.25 V vs. Pb/PbF₂, and a current density of 8 mA g⁻¹ was employed to evaluate the cycling stabilities at 140 °C.

3. Results and Discussion

3.1 Morphological changes after HPT processing

The XRD pattern of as-prepared PbSnF₄ was shown in Supplementary Fig. S2a. All the diffraction peaks were indexed to a β -structure with a space group of $P4_2/n$.¹⁷ The ionic conductivity of as-prepared PbSnF₄ is about 10⁻² S cm⁻¹ at 140 °C, which is also consistent with previous study (Supplementary Fig. S2b).¹⁷ To investigate the crystal structure of each component in the cathode composites after the HPT processing, we measured XRD patterns of the composites with different rotation numbers (N) of HPT processing (Fig. 2a). All peaks in the XRD pattern of the cathode composite without HPT processing (HPT-0) were indexed to Cu (space group: $Fm-3m$), PbSnF₄ (space group: $P4_2/n$), and Cu₂O impurity (space group: $Pn-3m$). After HPT processing, the peaks attributed to Cu were slightly broadened with the increase in N . The lattice parameters of Cu in the cathode composites were not changed with the increase in N (Supplementary Fig. S3), which indicates that the chemical composition of Cu was not changed after the HPT. In contrast to Cu in the cathode composite, the peaks attributed to PbSnF₄ were largely broadened. Particularly, the peaks attributed to PbSnF₄ almost disappeared for HPT-50. To evaluate the effects on the crystalline sizes of Cu and PbSnF₄ in the cathode composite with the HPT processing, we estimated each material's crystalline size by applying the Scherrer equation to the 220 peak of Cu and 102 peak of PbSnF₄ (Fig. 2b). The crystalline size of Cu was decreased from 35 to 15 nm from $N = 0$ to $N = 20$, and then was almost constant with the increase in N from 20 to 50. In contrast to Cu, the crystalline size of PbSnF₄ was largely decreased from 400 to 100 nm with the increase in N from 0 to 5, and then gradually decreased from 100 to 50 nm with the increase in N from 5 to 30. Finally, the crystalline size of PbSnF₄ was decreased to 20 nm in HPT-50.

The morphologies of the cathode composites before and after HPT with different anvil rotation numbers (N) were analyzed by SEM-EDX measurements. Figure 3 shows the EDX elemental mapping of the Cu-PbSnF₄-AB composite after the HPT treatment. The elemental maps of Sn and F exhibit similar tendencies to that of Pb; thus, the Pb-rich area can be regarded as PbSnF₄ phase. Before the HPT processing ($N = 0$), the PbSnF₄ secondary particles with sizes of a few micrometers were inhomogeneously distributed in the Cu matrix. Therefore, the locating Pb in the PbSnF₄ can be observed as the black part in the Cu mapping. With the increase in N to 10, the PbSnF₄ secondary particles became more fragmented into smaller particles due to the HPT deformation and finely distributed in the Cu matrix. In the samples with $N = 20$ and 30, the PbSnF₄ secondary

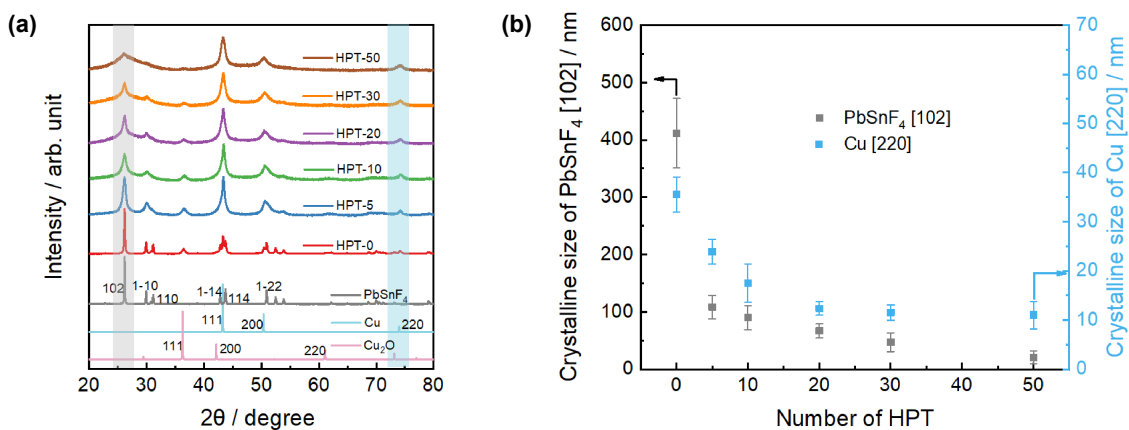


Figure 2. (a) XRD patterns and (b) crystalline sizes of Cu and PbSnF₄ in the cathode composites with different HPT rotation numbers. The crystalline sizes of Cu and PbSnF₄ were calculated by the PbSnF₄ [102] and Cu [220] peaks using the Scherrer's equation.

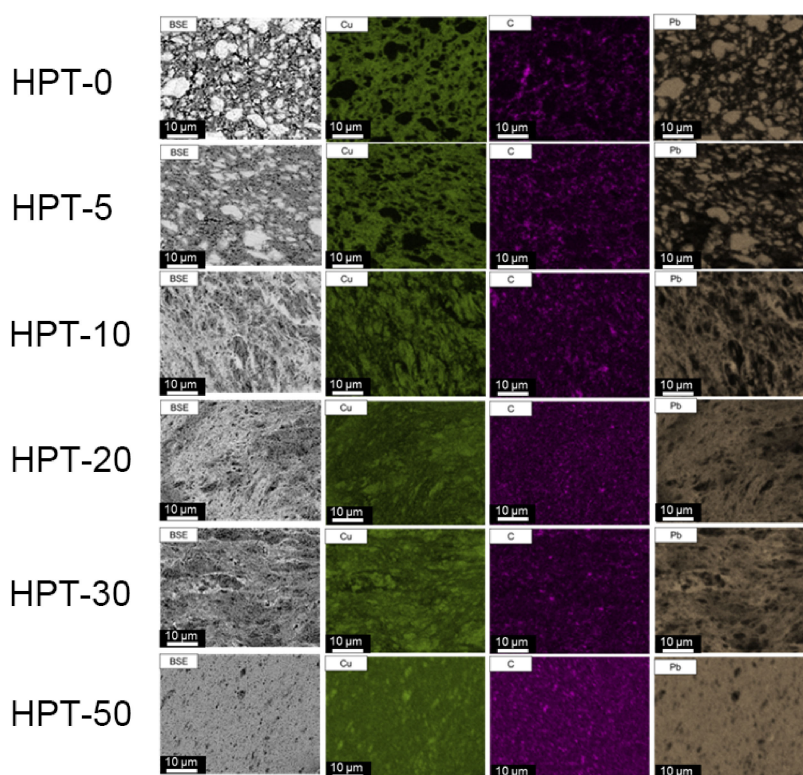


Figure 3. EDX mapping of the cathode composites after HPT processing with different anvil rotation numbers N .

particles became finer and more dispersed throughout the Cu active material. At $N = 50$, although the agglomerated Cu particles remained, the distribution of PbSnF₄ was very uniform, resulting in no black part of PbSnF₄ observed in Cu mapping. The carbon was uniformly distributed regardless of the degree of HPT. The SEM-EDX results indicate that, after the HPT processing, the secondary particle size of the solid electrolyte was significantly reduced and that Cu, PbSnF₄, and AB were more homogeneously distributed in the cathode composites.

3.2 Changes in the ionic conductivity with the HPT processing

To quantify the effect of the HPT processing on the fluoride-ion diffusion in the cathode composites, the fluoride-ion conductivity of the composite was measured using the electron blocking method. Figure 4a and Supplementary Fig. S4 show Nyquist plots for each cathode composite in the range of 25 to 125 °C. A half semicircle was observed in each composite's spectrum. The magnitude of the

semicircle decreased from $N = 0$ to $N = 40$, whereas it increased from $N = 40$ to $N = 50$. To quantitatively analyze the impedance spectra, the spectra were fitted with an equivalent circuit, as shown in Fig. 4b.²⁵ The obtained fitting parameters are shown in Supplementary Table S1. The semicircle was attributed to the grain boundary resistance because the obtained capacitance values of the semicircle in each spectrum were in the range of 10^{-11} to 10^{-8} F.²⁶ However, in the composite electrode, since the resistance of the interphase reaction between Cu and PbSnF₄ can be included in the semicircle, here we express the resistance as apparent grain boundary resistance. Arrhenius plots of the apparent grain boundary resistance and activation energies calculated by the plots for each cathode composite are shown in Figs. 4c and 4d.

The ionic conductivity of the apparent grain boundary was increased, while its activation energy was decreased from $N = 0$ to $N = 30$, as the crystalline sizes of Cu and PbSnF₄ were reduced (Fig. 2) and Cu, PbSnF₄, and AB were more homogeneously

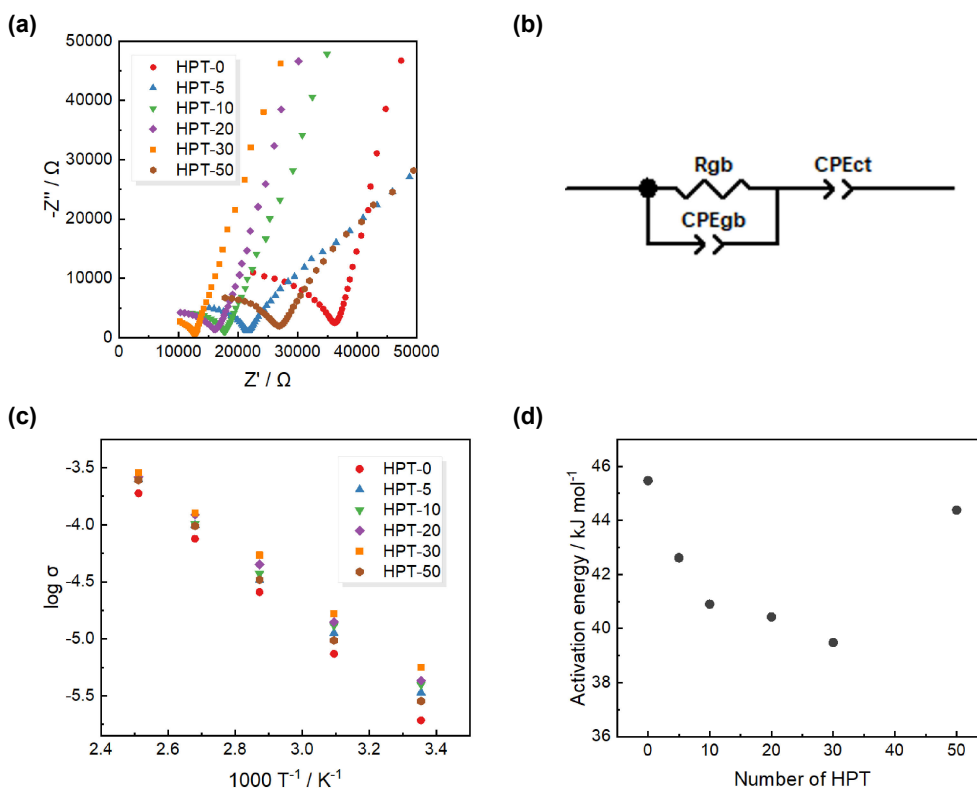


Figure 4. (a) Nyquist plots at 25 °C for the cathode composite after the HPT processing with different rotation numbers. (b) Equivalent circuit used for the electrochemical impedance spectroscopy (EIS) fitting. (c) Arrhenius plots for the ionic conductivity of the apparent grain boundary in the cathode composite with the HPT processing: $\log \sigma$ vs. $1000 T^{-1}$. (d) Activation energy calculated by the results in (c).

distributed in the cathode composites with reduced particle sizes of PbSnF_4 (Fig. 3). In contrast to the behavior from $N = 0$ to $N = 30$, the ionic conductivity of the apparent grain boundary was decreased, and its activation energy was increased from $N = 30$ to $N = 50$. The ionic conductivity decreases from $N = 30$ to $N = 50$ likely owing to the amorphization of PbSnF_4 by excessive HPT processing (Fig. 2) as the ionic conductivity of a solid electrolyte is largely influenced by its crystallinity.²⁷

3.3 Electrochemical performance

The electrochemical performances of the cathode composites after HPT processing with different rotation numbers were analyzed by the galvanostatic charge/discharge method, as shown in Fig. 5 and Supplementary Fig. S5. For all cathode composites, a single plateau was observed around 0.8 V during charging and 0.6 V during discharging. The shapes of the charge/discharge curves were consistent with those of the previous studies.^{15,16,18,28} These results indicate that, regardless of the rotation number of the HPT treatment, the charge/discharge reactions of the cathodes proceed via the two-phase coexistence reaction of Cu/CuF_2 .¹⁵ Although the HPT process did not change the charge/discharge shapes of the cathode composites, it largely influenced the polarization and capacities during the charge/discharge process. As the rotation number increased from 0 (HPT-0) to 30 (HPT-30), the discharge capacity increased from 149 to 435 mA h g^{-1} with the decrease in the polarization. However, the further increase in the rotation number to 50 (HPT-50) led to a decay of the discharge capacity to 322 mA h g^{-1} accompanied by the increase in the polarization.

The discharge capacity was improved from HPT-0 to HPT-30 as the diffusion length in Cu was decreased by the reduction in the crystalline size of Cu¹⁶ and the uniform mixing of Cu and PbSnF_4 formed a good ionic conduction path to Cu in the cathode composite.¹⁸ On the other hand, the deteriorated discharge capacity from HPT-30 to HPT-50 may be due to the decrease of the apparent

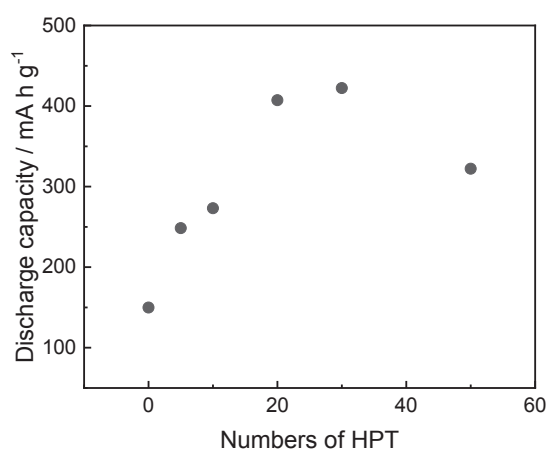


Figure 5. Discharge capacities of the cathode composites with different HPT rotation numbers at 0.01 C at 140 °C.

grain boundary ionic conductivity and electronic conductivity in the cathode composite due to the amorphization of the PbSnF_4 via excessive HPT processing. Composite electrodes with excellent electrochemical performances can be fabricated by an appropriate HPT treatment. As the HPT process can be applied to other active materials, this study provides important insights for future research on high-performance composite electrode design.

4. Conclusion

In this study, we applied HPT processing to prepare $\text{Cu}/\text{PbSnF}_4/\text{AB}$ cathode composites for all-solid-state FIBs, and analyzed their structures and electrochemical properties. Through the HPT processing, the Cu and PbSnF_4 particles were refined and uniformly

mixed each other in the cathode composites, resulting in a lower apparent grain boundary resistance than that of the cathode composite without HPT. However, PbSnF₄ was amorphized after the excessive HPT processing, resulting in an increase in the apparent grain boundary resistance. The cathode composite HPT-30, which underwent a suitable HPT processing, exhibited a significant discharge capacity (435 mA h g⁻¹), 2.5 times that of the cathode composite without HPT (149 mA h g⁻¹). These improvements were achieved as the diffusion length in Cu became small and the uniform mixing of Cu and PbSnF₄ formed a good ionic conduction path to Cu in the cathode composite via HPT processing. We believe that the HPT deformation, as a proven process for fabrication of composite electrodes, can have a propulsive role in the construction of high-energy-density all-solid-state FIBs.

Acknowledgment

This work was supported by JST-Mirai Program Grant Number JPMJMI18E2, Japan.

CRedit Authorship Contribution Statement

Yanchang Wang: Conceptualization (Equal), Data curation (Lead), Investigation (Lead), Writing – original draft (Lead)
 Sangmin Lee: Data curation (Lead), Methodology (Lead)
 Kentaro Yamamoto: Conceptualization (Equal), Investigation (Lead), Supervision (Lead), Writing – review & editing (Lead)
 Toshiyuki Matsunaga: Data curation (Supporting)
 Hidenori Miki: Data curation (Supporting), Methodology (Supporting), Project administration (Supporting)
 Hideki Iba: Methodology (Supporting), Project administration (Supporting)
 Koichi Tsuchiya: Data curation (Equal), Methodology (Lead), Project administration (Equal), Writing – review & editing (Supporting)
 Tomoki Uchiyama: Investigation (Supporting)
 Toshiki Watanabe: Investigation (Supporting)
 Tsuyoshi Takami: Investigation (Supporting)
 Yoshiharu Uchimoto: Project administration (Lead), Supervision (Lead), Writing – review & editing (Supporting)

Data Availability Statement

The data that support the findings of this study are openly available under the terms of the designated Creative Commons License in J-STAGE Data listed in D1 of References.

Conflict of Interest

The authors declare no conflict of interest in the manuscript.

Funding

Japan Science and Technology Corporation: JPMJMI18E2

References

- D1. Y. Wang, S. Lee, K. Yamamoto, T. Matsunaga, H. Miki, H. Iba, K. Tsuchiya, T. Uchiyama, T. Watanabe, T. Takami, and Y. Uchimoto, *J-STAGE Data*, <https://doi.org/10.50892/data.electrochemistry.21965774>, (2023).
- J. Janek and W. G. Zeier, *Nat. Energy*, **1**, 16141 (2016).
- J. Tarascon, *Electrochem. Soc. Interface*, **25**, 79 (2016).
- M. Armand and J.-M. Tarascon, *Nature*, **451**, 652 (2008).
- C. Delmas, J.-J. Braconnier, C. Fouassier, and P. Hagenmuller, *Solid State Ionics*, **3–4**, 165 (1981).
- Z. Jian, W. Luo, and X. Ji, *J. Am. Chem. Soc.*, **137**, 11566 (2015).
- D. Aurbach, Z. Lu, A. Schechter, Y. Gofer, H. Gizbar, R. Turgeman, Y. Cohen, M. Moshkovich, and E. Levi, *Nature*, **407**, 724 (2000).
- C. Xu, B. Li, H. Du, and F. Kang, *Angew. Chem., Int. Ed. Engl.*, **124**, 957 (2012).
- M.-C. Lin, M. Gong, B. Lu, Y. Wu, D.-Y. Wang, M. Guan, M. Angell, C. Chen, J. Yang, and B.-J. Hwang, *Nature*, **520**, 324 (2015).
- X. Zhao, Z. Zhao-Karger, D. Wang, and M. Fichtner, *Angew. Chem., Int. Ed. Engl.*, **52**, 13621 (2013).
- V. K. Davis, C. M. Bates, K. Omichi, B. M. Savoie, N. Momcilovic, Q. Xu, W. J. Wolf, M. A. Webb, K. J. Billings, N. H. Chou, S. Alayoglu, R. K. McKenney, I. M. Darolles, N. G. Nair, A. Hightower, D. Rosenberg, M. Ahmed, C. J. Brooks, T. F. Miller, R. H. Grubbs, and S. C. Jones, *Science*, **362**, 1144 (2018).
- M. Anji Reddy and M. Fichtner, *J. Mater. Chem.*, **21**, 17059 (2011).
- C. Rongeat, M. Anji Reddy, T. Diemant, R. J. Behm, and M. Fichtner, *J. Mater. Chem. A*, **2**, 20861 (2014).
- L. Zhang, M. A. Reddy, P. Gao, T. Diemant, R. Jürgen Behm, and M. Fichtner, *J. Solid State Electrochem.*, **21**, 1243 (2017).
- D. Zhang, H. Nakano, K. Yamamoto, K. Tanaka, T. Yahara, K. Imai, T. Mori, H. Miki, S. Nakanishi, H. Iba, T. Watanabe, T. Uchiyama, K. Amezawa, and Y. Uchimoto, *ACS Appl. Mater. Interfaces*, **13**, 30198 (2021).
- D. Zhang, K. Yamamoto, A. Ochi, Y. Wang, T. Yoshinari, K. Nakanishi, H. Nakano, H. Miki, S. Nakanishi, H. Iba, T. Uchiyama, T. Watanabe, K. Amezawa, and Y. Uchimoto, *J. Mater. Chem. A*, **9**, 406 (2021).
- T. Yoshinari, D. Zhang, K. Yamamoto, Y. Kitaguchi, A. Ochi, K. Nakanishi, H. Miki, S. Nakanishi, H. Iba, T. Uchiyama, T. Watanabe, T. Matsunaga, K. Amezawa, and Y. Uchimoto, *J. Mater. Chem. A*, **9**, 7018 (2021).
- D. Zhang, K. Yamamoto, Y. Wang, S. Gao, T. Uchiyama, T. Watanabe, T. Takami, T. Matsunaga, K. Nakanishi, H. Miki, H. Iba, K. Amezawa, K. Maeda, H. Kageyama, and Y. Uchimoto, *Adv. Energy Mater.*, **11**, 2102285 (2021).
- D. Zhang, T. Yoshinari, K. Yamamoto, Y. Kitaguchi, A. Ochi, K. Nakanishi, H. Miki, S. Nakanishi, H. Iba, T. Watanabe, T. Uchiyama, Y. Orikasa, K. Amezawa, and Y. Uchimoto, *ACS Appl. Energy Mater.*, **4**, 3352 (2021).
- M. A. Nowroozi, I. Mohammad, P. Molaiyan, K. Wissel, A. R. Munnangi, and O. Clemens, *J. Mater. Chem. A*, **9**, 5980 (2021).
- I. Sabirov, O. Kolednik, and R. Pippan, *Metall. Mater. Trans. A*, **36**, 2861 (2005).
- F. Meng, K. Tsuchiya, and Y. Yokoyama, *Intermetallics*, **37**, 52 (2013).
- G. Sakai, Z. Horita, and T. G. Langdon, *Mater. Sci. Eng. A*, **393**, 344 (2005).
- P. Vadhva, J. Hu, M. J. Johnson, R. Stocker, M. Braglia, D. J. L. Brett, and A. J. E. Rettie, *Chem. Electro. Chem.*, **8**, 1930 (2021).
- T. Asano, S. Yubuchi, A. Sakuda, A. Hayashi, and M. Tatsumisago, *J. Electrochem. Soc.*, **164**, A3960 (2017).
- A. Grenier, A. G. Porras-Gutierrez, M. Body, C. Legein, F. Chretien, E. Raymundo-Piñero, M. Dollé, H. Groult, and D. Dambournet, *J. Phys. Chem. C*, **121**, 24962 (2017).
- J. T. Irvine, D. C. Sinclair, and A. R. West, *Adv. Mater.*, **2**, 132 (1990).
- S. Yubuchi, H. Tsukasaki, A. Sakuda, S. Mori, A. Hayashi, and M. Tatsumisago, *RSC Adv.*, **9**, 14465 (2019).
- D. T. Thieu, M. H. Fawey, H. Bhatia, T. Diemant, V. S. K. Chakravadhanula, R. J. Behm, C. Kübel, and M. Fichtner, *Adv. Funct. Mater.*, **27**, 1701051 (2017).